JOURNAL OF SOLID STATE CHEMISTRY **141,** 352–364 (1998)
ARTICLE NO. SC987947

Structure, Chemical Bonding, Magnetic Susceptibility, and ^{155}Gd Mössbauer Spectroscopy of the Antiferromagnets GdAgGe, GdAuGe, $GdAu_{0.44(1)}In_{1.56(1)}$, and GdAuIn

Rainer Pöttgen and Gunter Kotzyba

Anorganisch-Chemisches Institut, Universität Münster, Wilhelm-Klemm-Straße 8, D-48149 Münster, Germany

Edward A. Görlich and Kazimierz Łątka,

Institute of Physics, Jagellonian University, Reymonta 4, 30-059 Kraków, Poland

and

Richard Dronskowski

Institut für Anorganische Chemie, RWTH Aachen, Professor-Pirlet-Straße 1, D-52056 Aachen, Germany

Received February 27, 1998; in revised form June 22, 1998; accepted June 29, 1998

DEDICATED TO PROFESSOR BERNT KREBS ON THE OCCASION OF HIS 60TH BIRTHDAY

GdAgGe, GdAuGe, $GdAu_{0.44(1)}In_{1.56(1)}$, and GdAuIn were prepared as single-phase materials from the elements by arc-melting and subsequent annealing at 970 K. The indium compounds were investigated by X-ray diffraction on both powders as well as single crystals. $GdAu_{0.44(1)}In_{1.56(1)}$ adopts the $CaIn_2$ structure, a puckered version of the AlB_2 type: $P6_3/mmc$, $a =$ 478.9(1) pm, $c = 740.3(1)$ pm, $V = 0.1470(1)$ nm^3, $Z = 2$, w$R2 =$ 0.0278, for 149 F^2 values, and 8 variables. GdAuIn crystallizes with a ternary ordered variant of the Fe_2P type: $P\bar{6}2m$, $a =$ 769.8(3) pm, $c = 397.8(2)$ pm, $V = 0.2042(1)$ nm^3, $Z = 3$, w$R2 =$ 0.0562, for 505 F^2 values, and 14 variables. GdAgGe crystallizes with the same structure, and GdAuGe adopts the NdPtSb type, a ternary ordered version of the $CaIn_2$ structure. Chemical bonding in GdAuIn was investigated by semiempirical band structure calculations. The strongest bonding interactions are found for the Au–In contacts, followed by Gd–Au and Gd–In, while the Gd–Gd interactions are much weaker. The four gadolinium compounds are antiferromagnets with Néel temperatures of 13.0, 16.9, 21.0, and 12.5 K for GdAgGe, GdAuGe, $GdAu_{0.44(1)}In_{1.56(1)}$, and GdAuIn, respectively. No field-induced magnetic transitions are evident from the low-temperature magnetization data. The magnetic hyperfine interactions in these intermetallics were studied in detail by ^{155}Gd Mössbauer spectroscopy. © 1998 Academic Press

Key Words: **crystal structure; antiferromagnetism; ^{155}Gd Mössbauer spectroscopy; chemical bonding.**

INTRODUCTION

The ternary systems rare earth metal (*RE*)–silver/gold–germanium/indium have been thoroughly examined in the past (1–5); however, the majority of these studies focused on phase analytical investigations. The Heusler-type phases REAg$_2$In and REAu$_2$In are the most intensively investigated compounds within these systems since they exhibit interesting physical properties (6). In contrast, little is known about the physical properties of the corresponding equiatomic compounds. Some remarkable examples of these compounds are the antiferromagnets CeAgGe (7) and CeAuIn (8) with Néel temperatures of 4.8 and 5.7 K, respectively, and the mixed-valence compound YbAuIn (9).

We have recently started a more systematic investigation on the crystal structures, the physical properties, and the chemical bonding of the REAgGe and REAuGe series (10–14). The most remarkable germanide herein is the 10.0 K ferromagnet CeAuGe (10, 11, 13). In the present study, we focus on the physical properties of the equiatomic gadolinium compounds GdAgGe, GdAuGe, and GdAuIn. The latter had only been characterized on the basis of X-ray powder data (1, 2). In addition, we report on the new compound $GdAu_{0.44(1)}In_{1.56(1)}$ which adopts the $CaIn_2$-type structure. The central topic of the present investigation is the study of the magnetic hyperfine interactions by magnetic

0022-4596/98 $25.00

susceptibility and ^{155}Gd Mössbauer spectroscopic measurements. Preliminary results of this work have been presented at a conference (15).

EXPERIMENTAL

Syntheses

Starting materials for the preparation of GdAgGe, GdAuGe, $GdAu_{0.44(1)}In_{1.56(1)}$, and GdAuIn were ingots of gadolinium (Johnson Matthey), silver wire (2 mm, Degussa), gold wire (1 mm, Degussa), germanium lumps (Wacker), and indium tear drops (Johnson Matthey), all with stated purities better than 99.9%. The large gadolinium ingots were cut into small pieces and kept under argon prior to the reactions. In a first reaction step, small gadolinium pieces were arc-melted under argon (about 600 mbar) in order to obtain compact buttons (about 400 mg). This preliminary melting process prevents a splashing of the ingots in the final reaction step. The argon had been purified before over molecular sieves, titanium sponge (900 K), and an oxisorb catalyst (16). In a second step, the elemental components were weighted in the ideal atomic ratio and placed into a water-cooled copper crucible. The elements were then reacted in an arc-furnace, and the resulting buttons were melted three times on each side to ensure homogeneity. The weight losses were smaller than 0.2% for each reaction. The products were subsequently sealed in evacuated quartz glass ampoules and annealed at 970 K for 20 days. Powders of GdAgGe, GdAuGe, $GdAu_{0.44(1)}In_{1.56(1)}$, and GdAuIn are dark gray, while single crystals (irregularly shaped; up to a size of 100 μm) are silvery with metallic lustre. The four compounds are stable in air over months. No decomposition, whatsoever, was observed.

X-Ray Investigations

Guinier powder patterns of the samples were recorded with Cu$K\alpha_1$ radiation. 5N silicon ($a = 543.07$ pm) was taken as an internal standard for the $GdAu_{0.44(1)}In_{1.56(1)}$ sample, while α-quartz ($a = 491.30$ pm, $c = 540.46$ pm) was taken for GdAgGe, GdAuGe, and GdAuIn. The powder patterns could easily be indexed on the basis of small hexagonal unit cells with those lattice constants listed in Table 1. No parasitic phases were observed on the Guinier patterns. To ensure correct indexing, the observed patterns were compared with calculated patterns (17) generated from the atomic positions of the structure refinements.

Single-crystal intensity data were collected by use of a four-circle diffractometer (CAD4) with graphite monochromatized Ag$K\alpha$ and Mo$K\alpha$ radiation for $GdAu_{0.44(1)}In_{1.56(1)}$ and GdAuIn, respectively, and a scintillation counter with pulse height discrimination.

Electronic Structure Calculations

A three-dimensional band structure calculation for GdAuIn was based on an extended Hückel Hamiltonian (18, 19), whereas off-site matrix elements were evaluated according to the weighted Wolfsberg–Helmholtz formula (20), minimizing counterintuitive orbital mixing.

The minimal orbital basis set was composed of Slater orbitals that had been fitted to *j*-averaged values of numerical Dirac–Fock functions. On-site Hamiltonian matrix elements were approximated by atomic orbital energies from the same source (21, 22). The values for the Gd 6*p* orbital are our estimates based on a number of atomic calculations for excited states of gadolinium. In detail, the exchange integrals (ξ orbital exponents in parentheses) were Gd 6*s*, −5.44 eV (1.52); Gd 6*p*, −3.84 (1.52); Gd 5*d*, −6.06 (2.03); Au 6*s*, −7.94 (2.12); Au 6*p*, −3.52 eV (1.53); In 5*s*, −10.79 eV (2.02), and In 5*p*, −5.35 (1.47). For obtaining greater accuracy, the Au 5*d* atomic wave functions (average orbital energy −12.55 eV) was approximated by a double-zeta function with exponents $\xi_1 = 4.20$, $\xi_2 = 1.86$ and weighting coefficients $c_1 = 0.814$, $c_2 = 0.336$ (23). The eigenvalue problem was solved in reciprocal space at 80 *k* points within the irreducible wedge of the Brillouin zone by using a modified EHMACC code (24).

Physical Properties

The magnetic susceptibilities of polycrystalline pieces of $GdAu_{0.44(1)}In_{1.56(1)}$ and GdAuIn were determined with

TABLE 1
Lattice Constants of the Hexagonal Compounds GdAgGe, GdAuGe, GdAuIn, and $GdAu_{0.44(1)}In_{1.56(1)}$

Compound	Str. type	*a* (pm)	*c* (pm)	*c*/*a*	*V* (nm^3)	Ref.
GdAgGe	ZrNiAl	715.4(2)	423.7(1)	0.592	0.1878(1)	12
GdAuGe	NdPtSb	442.64(2)	742.11(4)	1.677	0.12592(5)	13
GdAuIn	ZrNiAl	769.8(3)	397.8(2)	0.517	0.2042(1)	This work
GdAuIn	ZrNiAl	770.0	398.0	0.517	0.2044	1
GdAuIn	ZrNiAl	769.3(2)	399.1(1)	0.519	0.2046(1)	2
$GdAu_{0.44(1)}In_{1.56(1)}$	$CaIn_2$	478.9(1)	740.3(1)	1.546	0.1470(1)	This work

a MPMS SQUID magnetometer (Quantum Design, Inc.) from 4.2 to 300 K with magnetic flux densities up to 5.5 T.

The conventional constant acceleration spectrometer was used to perform Mössbauer absorption measurements for the 86.5 keV γ-transition of the ^{155}Gd isotope in the temperature range 4.2 to 30 K. The source was in the chemical form of (^{155}Eu)$SmPd_3$, and the quoted values of the isomer shifts are given relative to this material. The absorber thickness was optimized with respect to the best conditions for the signal to noise ratio. The theoretical shapes of the spectra were obtained as a set of Lorentzian lines whose positions and relative intensities resulted from diagonalization of the hyperfine Hamiltonian H_{hf}. The variable parameters of H_{hf} were the isomer shift, δ_{IS}, the coupling energy E_Q of the nuclear quadrupole moment eQ to the electric field gradient V_{zz}, the magnetic hyperfine field B_{hf}, the angle θ between the z axis of the electric field gradient and $\vec{B}_{hf}$ as well as the asymmetry parameter η and the azimuthal angle φ.

RESULTS AND DISCUSSION

Structure Refinements

Single crystals of $GdAu_{0.44(1)}In_{1.56(1)}$ and GdAuIn were isolated from the annealed samples by mechanical fragmentation and were examined by Buerger precession photographs in order to establish both symmetry and suitability for intensity data collection.

The needle-shaped crystal of GdAuIn was oriented with the needle axis perpendicular to the X-ray beam, and the axis turned out to be the short one, as is usually the case. The precession photographs (reciprocal layers $h0l$ and $h1l$) indicated hexagonal symmetry and showed no systematic extinctions. The structure refinements confirmed the noncentrosymmetric space group $P\bar{6}2m$, which is in agreement with previous investigations on isotypic compounds (12). The single crystals of $GdAu_{0.44(1)}In_{1.56(1)}$ were irregularly shaped. The reciprocal layers $h0l$ and $h1l$ indicated hexagonal symmetry. The systematic extinctions (hhl only observed with $l = 2n$) led to the space groups $P6_3/mmc$ and $P6_3mc$, of which the centrosymmetric group $P6_3/mmc$ was found to be correct during the structure refinement. All relevant crystallographic data and experimental details for the data collections are listed in Table 2.

The starting atomic parameters for both refinements were taken from an automatic interpretation of direct methods using SHELX-86 (25). The structures were then sucessfully refined using SHELXL-93 (26) with anisotropic atomic displacement parameters for all atoms. The 4*f* position of the $CaIn_2$ structure of $GdAu_{0.44(1)}In_{1.56(1)}$ was refined with a mixed occupancy by gold and indium atoms. In a separate

TABLE 2
Crystal Data and Structure Refinement for $GdAu_{0.44(1)}In_{1.56(1)}$ and GdAuIn

Empirical formula	$GdAu_{0.44(1)}In_{1.56(1)}$	GdAuIn
Formula weight	423.45 g/mol	469.04 g/mol
Temperature	293(2) K	293(2) K
Wavelength	56.086 pm (Ag$K\alpha$)	71.073 pm (Mo$K\alpha$)
Crystal system	hexagonal	hexagonal
Space group	$P6_3/mmc$ (No. 194)	$P\bar{6}2m$ (No.189)
Unit-cell dimensions	Table 1	Table 1
Formula units per cell	$Z = 2$	$Z = 3$
Calculated density	9.56 g/cm^3	11.45 g/cm^3
Crystal size	$35 \times 35 \times 55$ µm^3	$60 \times 60 \times 200$ µm^3
Absorption correction	from ψ-scan data	from ψ-scan data and DIFABS (27)
Transmission ratio (max/min)	1.52	3.85
Absorption coefficient	30.2 mm^{-1}	85.9 mm^{-1}
F(000)	351	576
θ range for data collection	2° to 27°	2° to 40°
Scan type	ω/θ	$\omega/2\theta$
Range in hkl	$0 \le h \le 7$, $-7 \le k \le 6$, $-11 \le l \le 11$	± 13, ± 13, ± 7
Total number of reflections	1202	2802
Independent reflections	149 ($R_{int} = 0.0595$)	505 ($R_{int} = 0.0778$)
Reflections with $I > 2\sigma(I)$	149 ($R_{sigma} = 0.0266$)	503 ($R_{sigma} = 0.0439$)
Refinement method	full-matrix least-squares on F^2	full-matrix least-squares on F^2
Data/restraints/parameters	127/0/8	505/0/14
Goodness-of-fit on F^2	1.289	1.252
Final R indices [$I > 2\sigma(I)$]	$R1 = 0.0169$, $wR2 = 0.0239$	$R1 = 0.0253$,$wR2 = 0.0560$
R indices (all data)	$R1 = 0.0272$, $wR2 = 0.0278$	$R1 = 0.0255$,$wR2 = 0.0562$
Extinction coefficient	0.0059(9)	0.0200(8)
Largest diff. peak and hole	1956 and -1812 e/nm^3	3082 and -3728 e/nm3
Absolute structure parameter	—	0.01(2)

series of least-squares cycles, the occupancy parameters for GdAuIn were varied along with the displacement parameters. No deviations from the ideal occupancies were observed. The anisotropic displacement parameters for GdAuIn, however, were extremly anisotropic with small U_{11} and U_{22} values and much larger U_{33} values. This anomaly was judged to be due to the needle-like shape of the crystal and strong absorption. The structure was then refined with isotropic displacement parameters, followed by a DIFABS absorption correction (27). The final refinement cycles were again carried out with anisotropic displacement parameters. The refined positional parameters before and after the DIFABS procedure were identical within less than one standard deviation. Final difference Fourier synthesis revealed no significant residual peaks for both refinements. The positional parameters, isotropic displacement parameters, and interatomic distances are listed in Tables 3 and 4. Further details on the structure refinements are available.[1]

TABLE 3
Atomic Coordinates and Isotropic Displacement Parameters (pm^2) for $GdAu_{0.44(1)}In_{1.56(1)}$ and GdAuIn

Atom	Wyckoff site	x	y	z	U_{eq}
		$GdAu_{0.44(1)}In_{1.56(1)}$, space group $P6_3/mmc$			
Gd	2*b*	0	0	1/4	99(2)
M	4*f*	1/3	2/3	0.04291(6)	138(1)
		GdAuIn, space group $P\bar{6}2m$			
Gd	3*f*	0.59365(9)	0	0	72(1)
Au1	1*a*	0	0	0	89(2)
Au2	2*d*	1/3	2/3	1/2	72(1)
In	3*g*	0.2589(1)	0	1/2	73(2)

Note. U_{eq} is defined as one third of the trace of the orthogonalized U_{ij} tensor. *M* denotes $Au_{0.88}In_{3.12}$.

Crystal Chemistry and Chemical Bonding

The new ternary alloy $GdAu_{0.44(1)}In_{1.56(1)}$ was obtained from a sample of the intended composition Gd : Au : In = 2 : 1 : 3 when searching for new intermetallic compounds with ordered structures derived from the simple AlB_2 type, such as Er_2RhSi_3 (28, 29) or U_2RuSi_3 (30, 31). The latter structures consist of slightly puckered Rh_2Si_4 and Ru_2Si_4 hexagons. Up to now, such ordered AlB_2 variants of the composition RE_2TX_3 have only been observed for silicides (28–31) and gallides (32, 33). These superstructures are the result of *klassengleiche* symmetry reductions (34), and give rise to additional reflections in the Guinier powder patterns. Our samples around the 2 : 1 : 3 composition revealed no superstructure reflections at all. $GdAu_{0.44(1)}In_{1.56(1)}$ crystallizes with the $CaIn_2$ structure, with the gadolinium atoms on the calcium position and a mixed occupancy of the gold and indium atoms on the indium position. Nevertheless, we would predict a large degree of short-range order in $GdAu_{0.44(1)}In_{1.56(1)}$. The structure of $GdAu_{0.44(1)}$ $In_{1.56(1)}$ is shown in Fig. 1. The gold and indium atoms form strongly puckered hexagons with average Au–In distances of 284 pm. This value compares well with the sum of Pauling's single-bond radii (35) of 283 pm for gold and indium. The average Au–In distances of 307 pm between the layers are much longer. We therefore assume stronger intralayer bonding and much weaker interlayer bonding within the three-dimensional $[Au_{0.44(1)}In_{1.56(1)}]$ polyanion. The puckering of the hexagons in $GdAu_{0.44(1)}In_{1.56(1)}$ is much more pronounced than within the structures of Er_2RhSi_3 (29) or U_2RuSi_3 (30).

At this point it is interesting to note that binary compounds with a $CaIn_2$ type structure are reported only for divalent cations like Ca, Sr, Eu, and Yb (36). A binary compound of the composition $GdIn_2$ is not known; however, the $CaIn_2$ type structure is realized for $GdAu_{0.44(1)}$ $In_{1.56(1)}$. Since the gold atoms are the most electronegative (assuming the Pauling scale) component in this compound we thus assume that the excess charge of trivalent gadolinium (as compared to divalent cations) is compensated by the electronegative gold atoms. The $CaIn_2$ type for $GdAu_xIn_{2-x}$ occurs if about 10% of the indium atoms are substituted by

TABLE 4
Selected Interatomic Distances (pm) in the Structures of $GdAu_{0.44(1)}In_{1.56(1)}$ and GdAuIn

$GdAu_{0.44(1)}In_{1.56(1)}$				GdAuIn			
Gd:	6	*M*	316.2	Gd:	4	Au2	306.8
	6	*M*	351.4		1	Au1	312.8
	2	Gd	370.1		2	In	325.5
					4	In	338.8
M:	3	*M*	283.7		2	Gd	397.8
	1	*M*	306.6		4	Gd	404.6
	3	Gd	316.2				
	3	Gd	351.4	Au1:	6	In	281.6
					3	Gd	312.8
				Au2:	3	In	289.5
					6	Gd	306.8
				In:	2	Au1	281.6
					2	Au2	289.5
					2	Gd	325.5
					4	Gd	338.8
					2	In	345.2

Note. Standard deviations are all equal or less than 0.1 pm. *M* denotes $Au_{0.22}In_{0.78}$.

[1]Details may be obtained from Fachinformationszentrum Karlsruhe, D-76344 Eggenstein-Leopoldshafen (Germany), by quoting the Registry Nos. CSD-410063 ($GdAu_{0.44(1)}In_{1.56(1)}$) and CSD-410064 (GdAuIn).

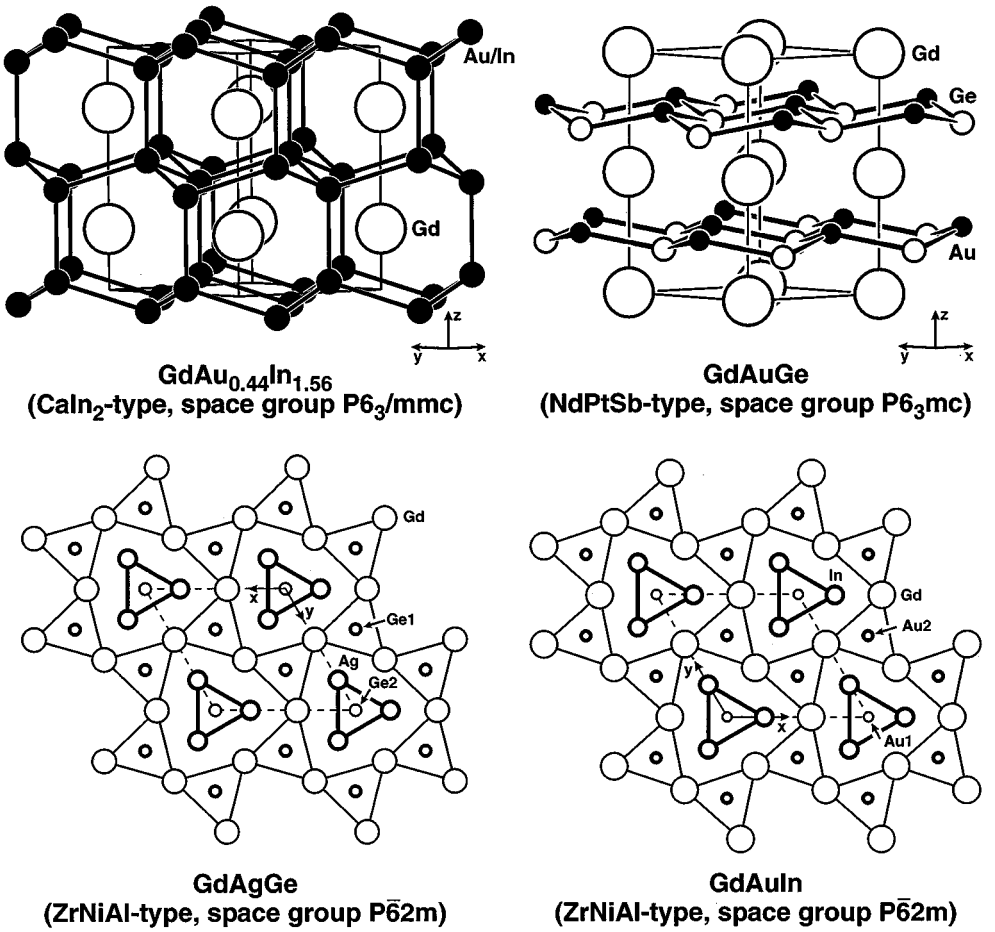

FIG. 1. Crystal structures of $GdAu_{0.44(1)}In_{1.56(1)}$, GdAuGe, GdAgGe, and GdAuIn. The structures of GdAgGe and GdAuIn are projected onto the *xy* plane, with all atoms on mirror planes at $z = 0$ and $z = 1/2$, indicated by thin and thick lines, respectively. The trigonal prisms around the germanium and gold atoms are outlined.

gold atoms. Arc-melted and annealed samples $GdAu_xIn_{2-x}$ with a lower gold content producted at Gd_3In_5 (36), $GdIn_3$ (36), and Au on the Guinier powder diagrams.

A completely ordered version of the $CaIn_2$ type is realized for GdAuGe (Fig. 1). The structure consists of puckered $[Au_3Ge_3]$ layers with strong covalent Au–Ge intralayer bonding and much weaker Au–Ge interlayer bonding. The gadolinium atoms are located within the polyanionic network. A detailed description of the crystal and electronic structures of *RE*AuGe intermetallics was recently given in (11) and (14).

Both GdAgGe and GdAuIn adopt the ZrNiAl-type structure, a ternary ordered version of Fe_2P (Figs. 1 and 2). These structures are also built up from two types of centered trigonal prisms, however, showing a different arrangement. In GdAgGe one type of these prisms is formed by the gadolinium atoms while the other type is formed by the silver atoms. Both prism types are centered by the smaller germanium atoms. A detailed discussion of the *RE*AgGe structures is given in (12). In GdAuIn, the prisms around the origin of the unit cell are formed by the indium atoms and centered by the smaller gold atoms. Thus, the positions of the transition metal and the *p* element are exchanged if compared to GdAgGe. In general, the trigonal prisms in Fe_2P-type compounds are always centered by the smaller atoms. The rectangular faces of the gold-centered indium prisms in GdAuIn are capped by three gadolinium atoms, while those of the gold-centered gadolinium prisms are capped by indium atoms, resulting in coordination number 9 (CN 9) for the gold atoms. Such a nearest neighbor environment with CN 9 is typically observed for transition-metal atoms in these intermetallic compounds.

The corresponding density-of-states (DOS) of GdAuIn in the valence region is presented in Fig. 3, indicating that the valence levels are heavily dominated by gadolinium *d* functions. The indium levels contribute to some degree at around -14 eV. The levels extending from -12 to -14 eV are mainly of Au *d* character.

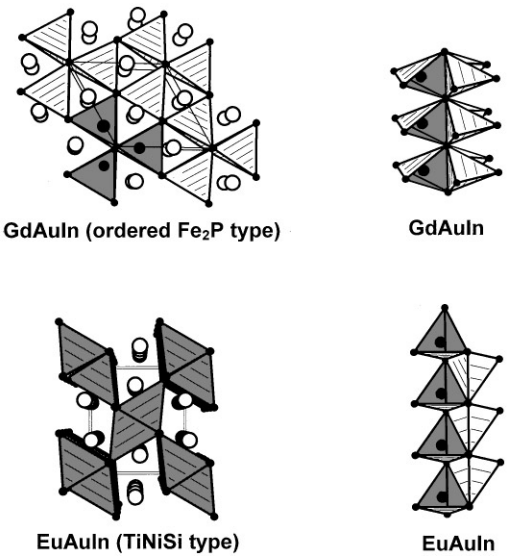

FIG. 2. Perspective views of the EuAuIn and GdAuIn structures along the x axis and the z axis, respectively, emphasizing the edge- and corner-sharing $InAu_4$ tetrahedra. Cutouts of smaller tetrahedral units are shown on the right-hand part. The shaded prisms in the drawing for GdAuIn correspond to the cutout presented at the upper right-hand part.

Chemical bonding in GdAuIn was investigated with the help of crystal orbital overlap populations (COOP) as presented in Fig. 4. The gold atoms form slightly distorted tetrahedra around the indium atoms with Au1–In and Au2–In distances of 282 and 290 pm, respectively, so that they agree excellently with the sum of Pauling's single-bond radii of 283 pm for gold and indium (35). The overlap population analysis (37) presented in Fig. 4 indeed confirms

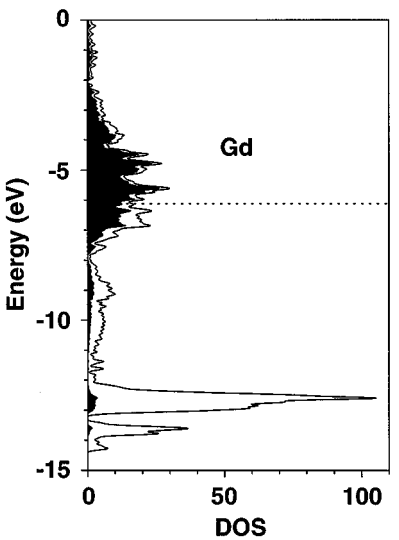

FIG. 3. Density-of-states (DOS) of GdAuIn with the gadolinium contributions emphasized in black.

these Au–In contacts to carry strong bonding character, with the highest overlap population of +0.288 in the GdAuIn structure. The Au–In bonding is seemingly optimized for the 17 valence electrons of GdAuIn with respect to the position of the Fermi level.

Short Au–In distances (283 to 288 pm) have also been observed recently for the $InAu_4$ tetrahedra in EuAuIn (38), adopting the TiNiSi-type structure. Although both compounds have a similar composition and tetrahedral $InAu_4$ units, there is a significant difference in structure and properties. There are always three tetrahedra in GdAuIn (ordered Fe_2P type) sharing common edges (Fig. 2) such that there results a propeller-like unit. These triple units are stacked onto each other along the z axis by sharing a common corner and forming one-dimensional infinite columns. The latter are condensed via common corners forming a three-dimensionally infinite [AuIn] polyanion in which the trivalent gadolinium atoms are embedded. Thus, each $InAu_4$ tetrahedron is condensed via one edge and all of its corners. In metamagnetic EuAuIn (38) the europium atoms are divalent and the $InAu_4$ tetrahedra have a higher degree of condensation: two common edges and all corners, as emphasized in Fig. 2. It is obvious that the structure of the [AuIn] polyanion strongly depends on the number of valence electrons transferred from the rare-earth element.

These structural features are nicely reflected by the recent results obtained for dimorphic YbPdSn (39). Here, the low-temperature modification (α-YbPdSn) contains trivalent ytterbium and adopts the ordered Fe_2P structure as does GdAuIn, while the high-temperature modification (β-YbPdSn) contains divalent ytterbium and crystallizes with the TiNiSi-type structure as does EuAuIn. Considering these findings one might assume a phase transition for EuAuIn: HT-EuAuIn (divalent europium, TiNiSi type) might possibly transform to LT-EuAuIn (trivalent europium, Fe_2P type). Such investigations are now in progress.

The shortest Gd–Gd distances in GdAuIn amount to 398 pm (equal to the length of the z axis), significantly longer than in *hcp* gadolinium (40), where each gadolinium atom has 12 nearest gadolinium neighbors with an average Gd–Gd distance of 360 pm. In a typical cluster compound like Gd_2Cl_3 (41, 42), where the gadolinium atoms form parallel chains of *trans* edge sharing Gd_6 octahedra, the Gd–Gd distances of 337 pm within the joined edges are much shorter. Such Gd–Gd interactions are strongly bonding. The very weak bonding character of the Gd–Gd interactions in GdAuIn is supported by the small Gd–Gd overlap population (+0.080, see also Fig. 4). Also, if the Gd–Gd interactions were of structural significance, one might have expected a slightly higher Fermi level (total electron count).

The five gold and six indium neighbors to gadolinium give rise to average Gd–Au and Gd–In distances of 308 and 334 pm, respectively, shorter than the sums of the metallic

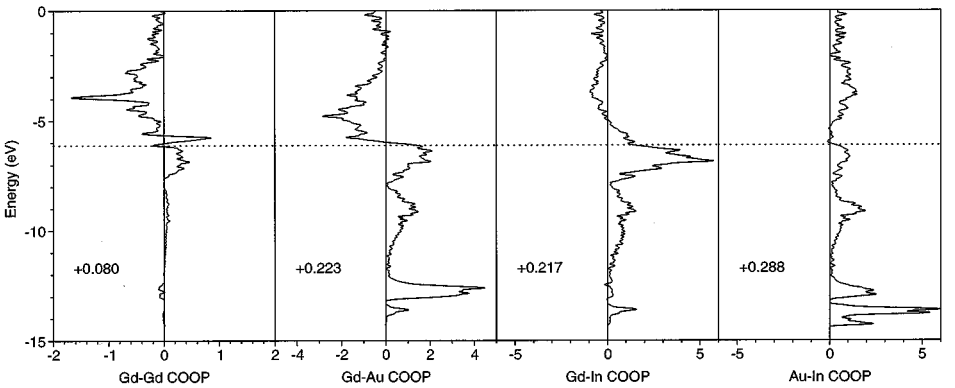

FIG. 4. Chemical bonding in GdAuIn from various crystal orbital overlap populations (COOP).

radii for CN 12 (43) of 324 pm (Gd–Au) and 347 pm (Gd–In). It is reasonable to assume mediate bonding interactions, which is in accordance with the overlap populations of +0.223 and +0.217, see also Fig. 4. Both Gd–Au and Gd–In interactions have significant contributions at the Fermi level.

Finally, it is worthwhile to note that the Fermi energy would touch the first Gd–Au antibonding levels within a rigid band model if additional electrons were inserted (Fig. 4), causing a structural destabilization. The removal of one electron, in contrast, should not significantly affect the stability of such an atomic arrangement. The validity of this rigid band model is nicely reflected by the existence of isotypic GdPtIn (44) with one electron less compared to GdAuIn and isoelectronic GdPtSn (45, 46). Both GdAuSn (1) and GdPtSb (46, 47), however, have one surplus electron and crystallize with the NdPtSb- and MgAgAs-type structure, respectively.

Magnetic Properties

The magnetic properties of GdAgGe and GdAuGe have been discussed in (12) and (13). Both germanides follow the Curie–Weiss law above 50 K. GdAgGe orders antiferromagnetically at 13.0(2) K and exhibits an experimental magnetic moment of $\mu_{exp} = 7.70\ \mu_B$ and a Weiss constant of −23(1) K. The gold compound orders antiferromagnetically at 16.9(2) K but with a reduced moment (compared to the free ion value of 7.94 μ_B) of $\mu_{exp} = 7.40\ \mu_B$ in the paramagnetic range. The Curie temperature is −2(1) K.

The temperature dependences of the inverse magnetic susceptibilities of GdAuIn and $GdAu_{0.44(1)}In_{1.56(1)}$ are shown in Figs. 5 and 6. Both compounds show Curie–Weiss behavior above 50 K, with experimental magnetic moments of $\mu_{exp} = 8.2(1)\ \mu_B$ and $\mu_{exp} = 7.8(1)\ \mu_B$ for GdAuIn and $GdAu_{0.44(1)}In_{1.56(1)}$, respectively. The paramagnetic Curie temperatures (Weiss constants) of −17(1) K for GdAuIn and −30(1) K for $GdAu_{0.44(1)}In_{1.56(1)}$ were obtained by linear extrapolations of the high-temperature parts of the $1/\chi$ vs T plots to $1/\chi = 0$. While the experimental magnetic moment for $GdAu_{0.44(1)}In_{1.56(1)}$ is slightly smaller than the free ion value of 7.94 μ_B for Gd^{3+}, the moment for GdAuIn is slightly enhanced, as is frequently observed for such equiatomic gadolinium compounds (6).

Antiferromagnetic ordering is observed at 12.5(5) K for GdAuIn and at 21.0(5) K for $GdAu_{0.44(1)}In_{1.56(1)}$ (insets of

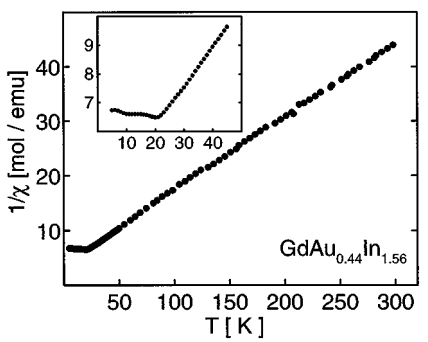

FIG. 5. Temperature dependence of the reciprocal magnetic susceptibility of $GdAu_{0.44(1)}In_{1.56(1)}$. The low temperature behavior is shown in the inset.

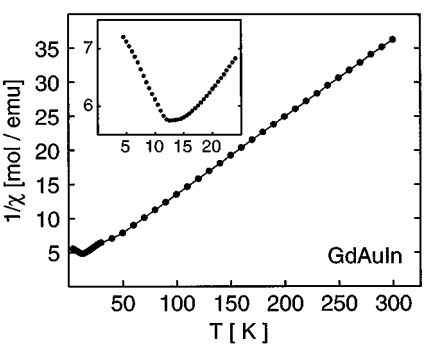

FIG. 6. Temperature dependence of the reciprocal magnetic susceptibility of GdAuIn. The low-temperature behavior is shown in the inset.

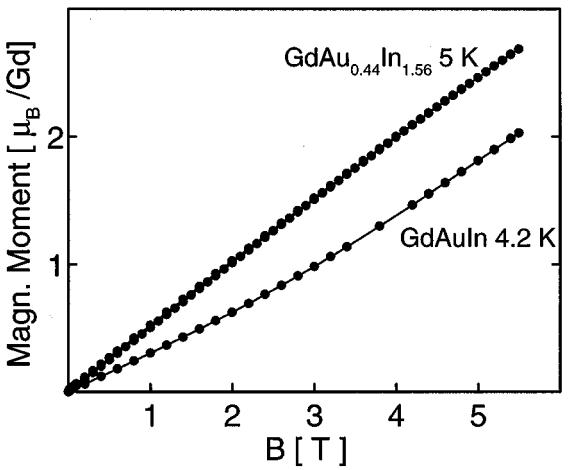

FIG. 7. Magnetization vs external magnetic flux density, B_{ext}, for $GdAu_{0.44(1)}In_{1.56(1)}$ and GdAuIn.

Figs. 5 and 6). The dependence of the magnetization vs the external magnetic flux density is shown in Fig. 7: they were evaluated at 4.2 K for GdAuIn and at 5 K for $GdAu_{0.44(1)}In_{1.56(1)}$. Both magnetization curves are more or less linear, as is expected for antiferromagnets. There is no hint of a field-induced magnetic transition. The magnetic moments at the highest obtainable external field strength of 5.5 T are 2.0(1) μ_B/Gd for GdAuIn and 2.6(1) μ_B/Gd for $GdAu_{0.44(1)}In_{1.56(1)}$, much smaller than the possible saturation value of 7.0 μ_B/Gd.

^{155}Gd Mössbauer Spectroscopy

Figures 8 through 11 show the experimental spectra as dots while the solid lines represent the least-squares fitted theoretical curves. The isomer shift is bound to the difference in electron density at the site of nucleus between the source and the absorber: $\delta_{IS} \sim \Delta\langle R_N^2\rangle(|\psi_A|^2 - |\psi_S|^2)$. The temperature variations of the isomer shifts seem to be statistically insignificant for all studied compounds (Fig. 12). Therefore, we have used the values averaged over the measured temperature range in order to characterize the samples. The isomer shift of ^{155}Gd in GdAuIn is distinctly smaller than for the remaining compounds under study. Since the quantity $\Delta\langle R_N^2\rangle$ (denoting the difference of the mean-squared radii of excited and ground nuclear states) is

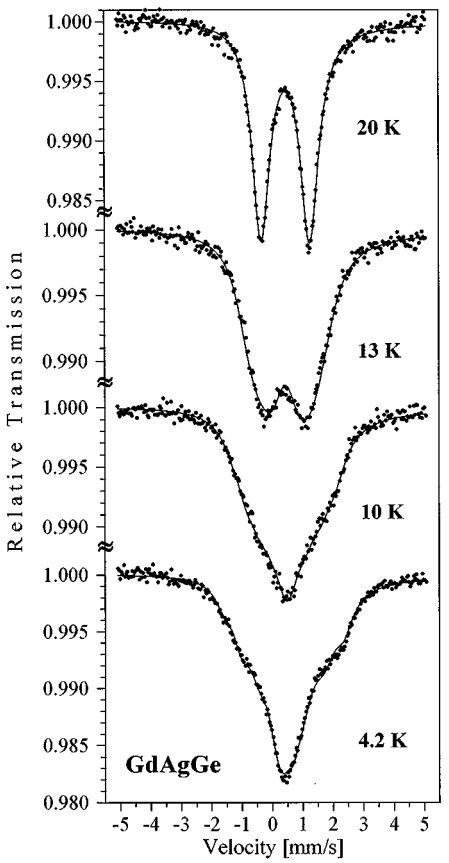

FIG. 8. Experimental and simulated ^{155}Gd Mössbauer spectra of GdAgGe at different temperatures.

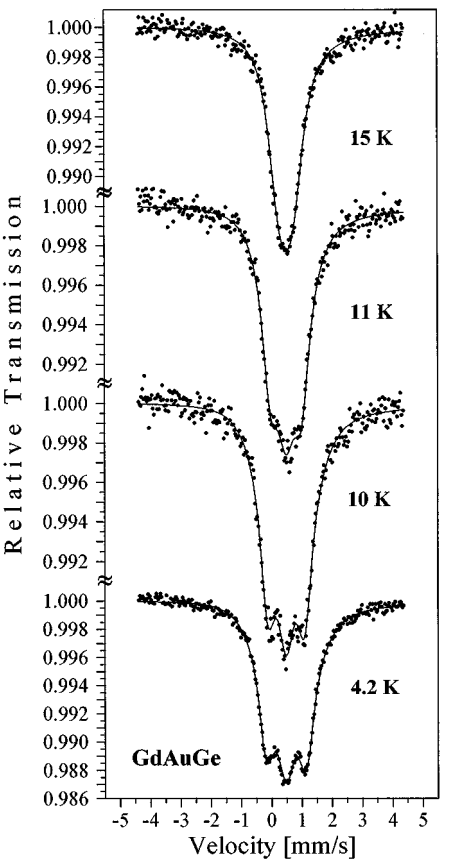

FIG. 9. Experimental and simulated ^{155}Gd Mössbauer spectra of GdAuGe at different temperatures.

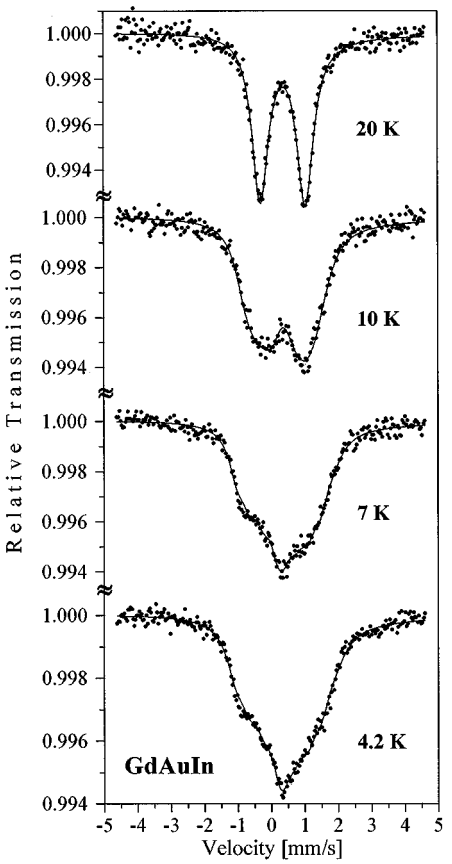

FIG. 10. Experimental and simulated ^{155}Gd Mössbauer spectra of GdAuIn at different temperatures.

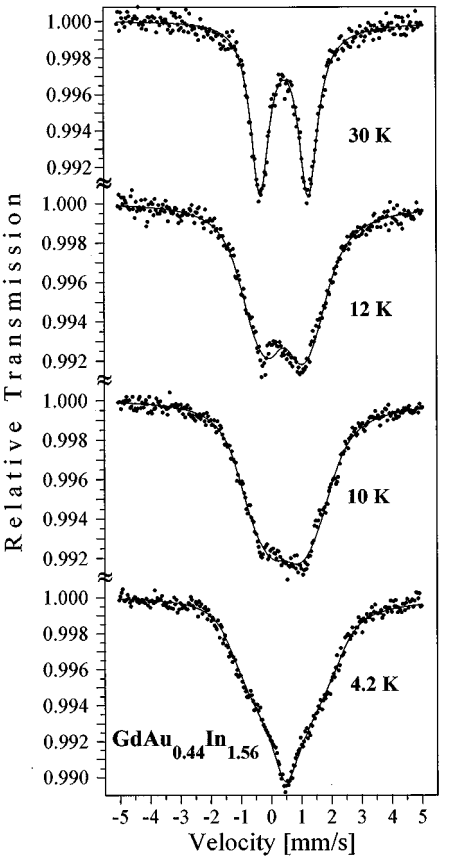

FIG. 11. Experimental and simulated ^{155}Gd Mössbauer spectra of $GdAu_{0.44(1)}In_{1.56(1)}$ at different temperatures.

negative for ^{155}Gd the electronic density $|\psi_A|^2$ at the gadolinium nucleus site must be higher in GdAuIn. The magnetic ordering temperatures that were determined from magnetic susceptibility and ^{155}Gd Mössbauer spectroscopic measurements (Table 5) agree rather well.

The important difference between the isomer shifts in the isostructural compounds GdAuIn and GdAgGe (Table 5) stems from a degree of *s* and *d* electrons rearrangement and may be derived from the details of gadolinium atom coordination in the two compounds. The gadolinium atom at the 3*f* Wyckoff position in GdAuIn (space group $\bar{P}62m$) is surrounded by a tetragonal pyramid of five gold atoms, the vertices of which are not all equivalent. The rectangular base of the pyramid is formed by four Au2 atoms at a distance of 307 pm from the central gadolinium atom (Table 4) while the "top" Au1 atom is 313 pm away (Fig. 1). The inversed occupation of the crystallographic sites between the transition metal and *p* element in GdAgGe (same ordered Fe_2P type structure) causes the new pyramid to be built of four basal Ge1 atoms with Ge2 at the apex (Fig. 1). The distances to the pyramid-centering gadolinium atom are 302 and 298 pm (12).

The results of the COOP calculations presented above supply a theoretical basis for the semiempirical model of Miedema and van der Woude (48) proposed for the interpretation of isomer shifts in binary intermetallic A_xB_y systems. This model uses the electronegativity difference $\Delta\phi^* \equiv \phi_B^* - \phi_A^*$ and the difference in electron densities taken at the boundaries of the Wigner–Seitz cells of pure metals $\Delta n_{WS} \equiv n_{WS}^B - n_{WS}^A$ as the basic physical properties determining the Mössbauer isomer shifts δ_{IS}^A of element *A* in A_xB_y relative to that of pure *A* (47): $\delta_{IS}^A \equiv f_B^A\ [P'\Delta\phi^* + Q'\Delta n_{WS}/n_{WS}^A]$.

The coordination fraction f_B^A accounts for the completeness of the surrounding of *A* and *B* atoms, and it proportionally reduces the maximum isomer shift which would have been observed in the case of infinite dilution of *A* in *B*. The f_B^A fraction depends on the concentration of *A* in *B*, their relative atomic sizes, and the coordination geometry. The constants P' and Q' are obtained by optimizing an agreement between the isomer shifts calculated from the above formula and those measured for a series of compounds. The approach was also applied for the analysis of ^{155}Gd isomer shifts (49) as well as adapted to ternary gadolinium

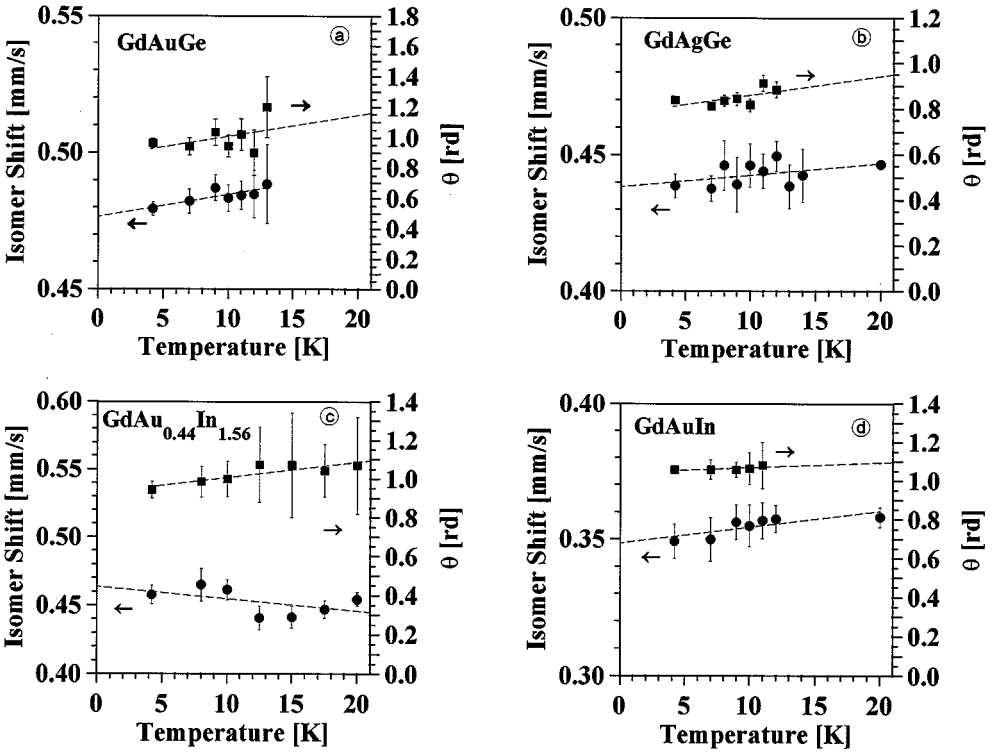

FIG. 12. Temperature dependencies of the isomer shifts and the angle θ (between the z axis of the electric field gradient and $\vec{B}_{hf}$) for GdAgGe, GdAuGe, GdAuIn, and $GdAu_{0.44(1)}In_{1.56(1)}$.

compounds (50). For ^{155}Gd the values $P' = 0.27$ mm/s and $Q' = -0.11$ mm/s were determined from measurements for a series of gadolinium-transition metal compounds (49).

The strong d electron transfer from the gadolinium to the gold sites considerably decreases the shielding of gadolinium s character electrons, thus increasing their density at the gadolinium nuclei. The high Gd–Au overlap population of +0.223 in GdAuIn confirms the bonding interactions. As indicated above, the average Gd–Au distance is shorter than the sum of their metallic radii. The average Gd–Ge distance in GdAgGe (300 pm) (12) is also smaller than the sum of the respective metallic radii (317 pm); however, taking into account a considerably smaller difference in electronegativities between the latter elements than in the case of Gd–Au one might expect a much smaller d electron transfer away from the gadolinium site.

TABLE 5
^{155}Gd Mössbauer Parameters for GdAgGe, GdAuGe, GdAuIn, and $GdAu_{0.44(1)}In_{1.56(1)}$

Compound	δ_{IS}[a] (mm/s)	E_Q[b] (mm/s)	θ (deg)	$B_{hf}(0)$[c] (T)	T_{ord} (K)	T_{mag}[f] (K)
GdAgGe	0.443(4)	−0.841(3)	52(5)	26.8(2)	14.8(2)	13.0(2)
GdAuGe	0.484(3)	−0.110(40)	58(5)	26.6(1)	16.0(2)	16.9(2)
GdAuIn	0.355(4)	−0.707(4)	61(5)	18.4(2)	12.2(2)	12.5(5)
$GdAu_{0.44(1)}In_{1.56(1)}$	0.452(10)	−0.842(4)	59(3)	19.8(1)[d]	24.5(5)[e]	21.0(5)

[a] The average value in a measured temperature range.

[b] Electric quadrupole coupling $E_Q \equiv 1/4eQV_{zz}$ of the nuclear moment eQ with a field gradient V_{zz}. The values were obtained from the spectra above T_{ord}. The sign was inferred from magnetically split spectra. For the 86.5 keV Mössbauer transition in ^{155}Gd, 1 mm/s corresponds to 69.803 MHz.

[c] Saturation value resulting from the fitted molecular field $S = 7/2$ dependence.

[d] The value measured at 4.2 K.

[e] The value linearly extrapolated from the B_{hf} vs T dependence.

[f] The magnetic ordering temperatures T_{mag} as determined from susceptibility measurements are listed for comparison.

The nuclear electric quadrupole energy E_Q results from the coupling of the nuclear moment eQ to nonspherical charge distributions described by the electric field gradient (EFG) tensor (of main z-component V_{zz}): $E_Q \equiv 1/4eQV_{zz}$. For the S-state ion Gd^{3+} the otherwise ($L \neq 0$) dominant $4f$ contribution is absent and the EFG tensor is determined by the charge arrangement in the crystal lattice modified by screening effects of core, valence, and conduction electrons. In all cases, the quadrupole coupling constant, E_Q, is negative. The absolute value was somewhat lower for GdAuIn and distinctly lower for GdAuGe than for the remaining compounds, as may readily be seen from the spectra (Figs. 8–11). The asymmetry parameter η, as defined by the main components of the electric field gradient tensor $\eta \equiv (V_{yy} - V_{xx})/V_{zz}$ with the convention $|V_{zz}| \geq |V_{yy}| \geq |V_{xx}|$ was determined from the low-temperature spectra of GdAuIn to lie around 0.6(1). This may be expected for gadolinium occupying the $3f$ site of *mm* site symmetry in the ordered Fe_2P-type structure. For reasons of symmetry, one may assume that the main z axis of a local system diagonalizing the electric field gradient tensors at the gadolinium nuclei remains in the basal plane ($\perp$**c**), pointing toward the Au1 pyramidal apex. For other samples practically no deviation from the axial symmetry of EFG was observed, i.e., $\eta = 0.0(1)$. The parameters V_{zz} and η obtained from ^{155}Gd Mössbauer spectra are useful in that they can provide estimates for the quadrupolar terms B_2^0 and B_2^2 in the Stevens expansion $\Sigma B_n^m O_n^m$ of a crystal field; for a rare-earth $4f$ shell with nonzero orbital angular momentum, an appropriate Stevens factors α_J (51) and an expectation value of the squared $4f$ radius $\langle r^2 \rangle_{4f}$ (52) one arrives at

$$B_2^0 = -\alpha_j \cdot \langle r^2 \rangle_{4f} \cdot \frac{e(1-\sigma_2)}{4(1-\gamma_\infty)} V_{zz} \quad \text{and} \quad B_2^2 = \eta \cdot B_2^0,$$

where σ_2 and γ_∞ account for screening effects. The values of these shielding factors are difficult to determine reliably in particular for metallic systems but information about the sign of B_2^0 may usually be gained. The value presently accepted as a reasonable estimate of the screening factors ratio $[(1-\sigma_2)/(1-\gamma_\infty)]^{-1}$ for the rare earth is 200 (53). Another source of quantitative uncertainty is connected with the value of the ground state ^{155}Gd quadrupole moment Q; it is needed in order to calculate the electric field gradient V_{zz} component from the measured quadrupole coupling energy E_Q defined above. The most reliable value of Q seems to be 1.30(2) as measured in the muonic X-ray experiment (54). Summarizing, the practical formula, to estimate the B_2^0 coefficient (expressed in [K]) from the nuclear quadrupole coupling constant E_Q (given in [mm/s] of the 86.5 keV transition in ^{155}Gd (Table 5)) reads: B_2^0[K] $= -\alpha_J \cdot \langle r^2 \rangle_{4f} \cdot 361 \cdot E_Q$. The numerical factor corresponds to $\langle r^2 \rangle_{4f}$ values expressed in squared atomic units a_o^2 as given in (52).

The main contributions to the magnetic hyperfine field B_{hf} at the gadolinium nucleus arise from s-electron polarization (both core and conduction) by the spin magnetic moment of the Gd^{3+} ion itself as well as by the neighboring lattice moments (transferred field, RKKY-type mechanism). The core-polarization component of the local field amounts to $-34(2)$ T (negative since it is opposite to the direction of the local $4f$ moment) and it is almost independent from the environment of the gadolinium atoms. In compounds where only gadolinium carries a magnetic moment, B_{hf} is proportional to the expectation value $\langle S_z \rangle$. In the present cases, the temperature dependencies of B_{hf} were found to conform with the Brillouin function $S = 7/2$ behavior (Fig. 13). The higher net electronic density at the gadolinium nuclear site in GdAuIn deduced from the isomer shift values may account for the smaller absolute value of the saturation hyperfine field, B_{hf}, encountered there (Table 5, Figs. 11 and 13). This is accomplished by an increased positive transfered field which adds to the negative core contribution. A rather unusual and very interesting temperature dependence of $|B_{hf}|$ in $GdAu_{0.44(1)}In_{1.56(1)}$ (Fig. 14) may arise from the specific way of a percolative demagnetization process at intermediate temperatures, magnetically ordered and disordered (or differently ordered) regions coexist in temperature-dependent proportions. However, the spectrum could still be described with a single hyperfine pattern such that an effective averaging over the different local magnetic surroundings of the gadolinium nuclei exists. In fact, the strongly enhanced experimental line width ($\Gamma_{exp} = 1.20$ mm/s, the other investigated phases are close to 0.85 mm/s) indicates an inequivalence of gadolinium sites with respect to hyperfine interactions. The described behavior is also consistent with a situation in which the magnetic

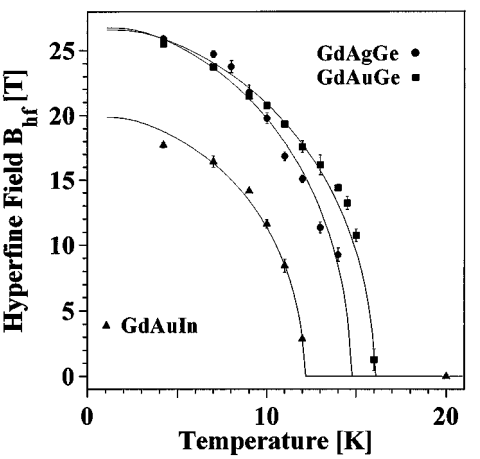

FIG. 13. Temperature dependence of the internal magnetic hyperfine fields B_{hf} of GdAgGe, GdAuGe, and GdAuIn.

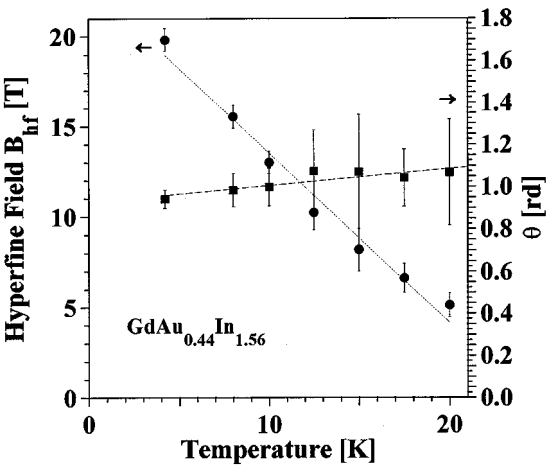

FIG. 14. Temperature dependence of the magnetic hyperfine field B_{hf} and the angle θ (between the z axis of the electric field gradient and $\vec{B}_{hf}$) for $GdAu_{0.44(1)}In_{1.56(1)}$.

ordering has a spin-glass character (55). Extreme low-field magnetic susceptibility measurements may shed light on the problem. In higher magnetic fields, the $GdAu_{0.44(1)}In_{1.56(1)}$ sample exhibits regular antiferromagnetic properties (Figs. 5 and 7). The random distribution of gold and indium atoms over the indium site of this $CaIn_2$ type compound may favor such a behavior.

The angle θ between the direction of the hyperfine field (and thus of the gadolinium magnetic moment) and the principal axis of the electric field gradient (EFG) tensor does not differ significantly among the compounds, and it is close to 1 rd (57°) (Table 5). If the orientation of the EFG principle axis were known, it would be possible to determine the direction of the easy magnetic axis.

CONCLUSIONS

The antiferromagnets GdAgGe, GdAuGe, $GdAu_{0.44(1)}In_{1.56(1)}$, and GdAuIn have been prepared as single-phase materials and their structures have been investigated by X-ray diffraction techniques. $GdAu_{0.44(1)}In_{1.56(1)}$ adopts the $CaIn_2$ structure, GdAgGe and GdAuIn crystallize with a ternary ordered variant of the Fe_2P type, and GdAuGe adopts the NdPtSb type. Chemical bonding in GdAuIn was investigated by semiempirical band structure calculations. The strongest bonding interactions are found for the Au–In contacts, followed by Gd–Au and Gd–In. The four gadolinium compounds are antiferromagnets with Néel temperatures of 13.0, 16.9, 21.0, and 12.5 K for GdAgGe, GdAuGe, $GdAu_{0.44(1)}In_{1.56(1)}$, and GdAuIn, respectively. No field-induced magnetic transitions are evident from the low-temperature magnetization data. The magnetic hyperfine interactions in these intermetallics were studied in detail by ^{155}Gd Mössbauer spectroscopy.

ACKNOWLEDGMENTS

We thank Professor Wolfgang Jeitschko for his interest and steady support. We are also indebted to Dr. Horst Borrmann and Dr. Manfred H. Möller for the collections on the four-circle diffractometer data, to Eva Brücher and Dr. Reinhard K. Kremer for the susceptibility measurement of $GdAu_{0.44(1)}In_{1.56(1)}$, and to Dr. Wolfgang Gerhartz (Degussa AG) for a generous gift of gold and silver wire. This work was financially supported by the Deutsche Forschungsgemeinschaft (Po573/2-1), the Fonds der Chemischen Industrie, and by the Polish State Committee for Scientific Research (Grant 2 P03B 116 12).

REFERENCES

1. A. E. Dwight, in "Proceedings of the Rare Earth Research Conference, 12th, Colorado," Vol. 1, p. 480, 1976.
2. D. Rossi, R. Ferro, V. Contardi, and R. Marazza, *Z. Metallkd.* **68,** 493 (1977).
3. R. Marazza, R. Ferro, and D. Rossi, *Z. Metallkd.* **66,** 110 (1975).
4. G. Zanicchi, D. Mazzone, V. Contardi, R. Marazza, G. Rambaldi, and D. Rossi, *Gazz. Chim. Ital.* **113,** 257 (1983).
5. D. Rossi, R. Marazza, and R. Ferro, *J. Alloys Compd.* **187,** 267 (1992).
6. A. Szytula and J. Leciejewicz, "Handbook of Crystal Structures and Magnetic Properties of Rare Earth Intermetallics," CRC Press, Boca Raton, FL, 1994.
7. V. K. Pecharsky, K. A. Gschneidner Jr., O. I. Bodak, and A. S. Protsyk, *J. Less-Common Met.* **168,** 257 (1991).
8. H. Fujii, Y. Uwatoko, M. Akayam, K. Satch, Y. Maeno, T. Fujita, J. Sakurai, H. Kamimura, and T. Okamoto, *Jpn. J. Appl. Phys.* **26,** 549 (1987).
9. W. Zell, R. Pott, B. Roden, and D. Wohlleben, *Solid State Commun.* **40,** 751 (1981).
10. R. Pöttgen, H. Borrmann, and R. K. Kremer, *J. Magn. Magn. Mater.* **152,** 196 (1996).
11. R. Pöttgen, H. Borrmann, C. Felser, O. Jepsen, R. Henn, R. K. Kremer, and A. Simon, *J. Alloys Compd.* **235,** 170 (1996).
12. B. Gibson, R. Pöttgen, R. K. Kremer, A. Simon, and K. R. A. Ziebeck, *J. Alloys Compd.* **239,** 34 (1996).
13. B. J. Gibson, W. Schnelle, R. Pöttgen, K. Bartkowski, and R. K. Kremer, *Czech J. Phys.* **46,** S5, 2573 (1996).
14. W. Schnelle, R. Pöttgen, R. K. Kremer, E. Gmelin, and O. Jepsen, *J. Phys. Cond. Matter* **9,** 1435 (1997).
15. R. Pöttgen and Y. Grin, *Z. Kristallogr.* Suppl. **12,** 136 (1997).
16. H. L. Krauss and H. Stach, *Z. Anorg. Allg. Chem.* **366,** 34 (1969).
17. K. Yvon, W. Jeitschko, and E. Parthé, *J. Appl. Crystallogr.* **10,** 73 (1977).
18. R. Hoffmann, *J. Chem. Phys.* **39,** 1397 (1963).
19. Roald Hoffmann, "Solids and Surfaces: A Chemist's View of Bonding in Extended Structures," VCH, Weinheim, New York, 1988.
20. J. H. Ammetter, H.-B. Bürgi, J. C. Thibeault, and R. Hoffmann, *J. Am. Chem. Soc.* **100,** 3686 (1978).
21. J. P. Desclaux, *At. Data Nucl. Data Tables* **12,** 3110 (1973).
22. P. Pyykkö and L. L. Lohr, Jr., *Inorg. Chem.* **20,** 1950 (1981).
23. N. J. Fitzpatrick and G. H. Murphy, *Inorg. Chim. Acta* **111,** 139 (1986).
24. M. H. Whangbo, M. Evain, T. Hughbanks, M. Kertesz, S. Wijeyesekera, C. Wilker, C. Zheng, and R. Hoffmann, QPCE program EHMACC.
25. G. M. Sheldrick, "SHELX-86, Program for the Solution of Crystal Structures," University of Göttingen, Germany, 1986.
26. G. M. Sheldrick, "SHELXL-93, Program for Crystal Structure Refinement," University of Göttingen, Germany, 1993.
27. N. Walker and D. Stuart, *Acta Crystallogr. Sect. A* **39,** 158 (1983).

28. B. Chevalier, P. Lejay, J. Etourneau, and P. Hagenmuller, *Solid State Commun.* **49,** 753 (1984).
29. R. E. Gladyshevskii, K. Cenzual, and E. Parthé, *J. Alloys Compd.* **189,** 221 (1992).
30. R. Pöttgen, P. Gravereau, B. Darriet, B. Chevalier, E. Hickey, and J. Etourneau, *J. Mater. Chem.* **4,** 463 (1995).
31. B. Chevalier, R. Pöttgen, B. Darriet, P. Gravereau, and J. Etourneau, *J. Alloys Compd.* **233,** 150 (1996).
32. Ch. D. Routsi, J. K. Yakinthos, A. Garnier, D. Gignoux, F. Lionti, and D. Schmitt, *J. Alloys Compd.* **240,** 151 (1996).
33. V. H. Tran, D. Kaczorowski, T. Roisnel, R. Troc, H. Noël, F. Bourrée, and. G. André, *Physica B* **205,** 24 (1995).
34. J. H. Albering, R. Pöttgen, W. Jeitschko, R.-D. Hoffmann, B. Chevalier, and J. Etourneau, *J. Alloys Compd.* **206,** 133 (1994).
35. L. Pauling, "The Nature of the Chemical Bond and The Structures of Molecules and Crystals," Cornell Univ. Press, Ithaca, NY, 1960.
36. P. Villars and L. D. Calvert, "Pearson's Handbook of Crystallographic Data for Intermetallic Phases," second edition, American Society for Metals, Materials Park, OH, 1991.
37. T. Hughbanks and R. Hoffmann, *J. Am. Chem. Soc.* **105,** 3528 (1983).
38. R. Pöttgen, *J. Mater. Chem.* **6,** 63 (1996).
39. D. Kußmann, R. Pöttgen, B. Künnen, R. Müllmann, B. D. Mosel, and G. Kotzyba, *Z. Kristallogr.* **213,** 356 (1998).
40. J. Donohue, "The Structures of the Elements," Wiley, New York, 1974.
41. D. A. Lokken and J. D. Corbett, *Inorg. Chem.* **12,** 556 (1973).
42. A. Simon, N. Holzer, and Hj. Mattausch, *Z. Anorg. Allg. Chem.* **456,** 207 (1979).
43. E. Teatum, K. Gschneidner Jr., and J. Waber, Rep. LA-2345, US Department of Commerce, Washington, DC, 1960.
44. R. Ferro, R. Marazza, and G. Rambaldi, *Z. Anorg. Allg. Chem.* **410,** 219 (1974).
45. A. E. Dwight, W. C. Harper, and C. W. Kimball, *J. Less-Common Met.* **30,** 1 (1973).
46. J. W. C. de Vries, R. C. Thiel, and K. H. J. Buschow, *J. Less-Common Met.* **111,** 313 (1985).
47. A. E. Dwight, in "Proc. Rare Earth Res. Conf., 11th, Michigan," Vol. 2, p. 642, 1974.
48. A. R. Miedema and F. van der Woude, *Physica B* **100,** 145 (1980).
49. H. de Graaf, R. C. Thiel, and K. H. J. Buschow, *J. Phys. F* **12,** 2079 (1982).
50. J. W. C. de Vries, R. C. Thiel, and K. H. J. Buschow, *J. Less-Common Met.* **111,** 313 (1985).
51. K. R. Lea, M. J. M. Leask, and W. P. Wolf, *J. Phys. Chem. Solids* **23,** 1381 (1962).
52. A. J. Freeman and J. P. Desclaux, *J. Magn. Magn. Mater.* **12,** 11 (1979).
53. G. Czjzek *in* "Mössbauer Spectroscopy Applied to Magnetism and Materials Science," (G. J. Long and F. Grandjean, Eds.) Vol. 1, p. 373, Plenum Press, New York, 1993.
54. Y. Tanaka, D. B. Laubacher, R. M. Steffen, E. B. Shera, H. D. Wohlfahrt, and M. V. Hoehn, *Phys. Lett. B* **108,** 8 (1982).
55. K. Łątka, E. A. Görlich, W. Chajek, R. Kmieć, and A. W. J. Pacyna, *J. Alloys Compd.* **262–263,** 108 (1997).